ACS APPLIED MATERIALS & INTERFACES

Research Article

www.acsami.org

Hierarchically Structured ZnO Nanorods–Nanosheets for Improved Quantum-Dot-Sensitized Solar Cells

Jianjun Tian,*[,†] Evan Uchaker,[‡] Qifeng Zhang,[‡] and Guozhong Cao*[,‡,§]

[†]Advanced Materials Technology Institute, University of Science and Technology Beijing, Beijing 100083, China

[‡]Department of Materials Science & Engineering, University of Washington, Seattle, Washington 98195, United States

[§]Beijing Institute of Nanoenergy and Nanosystems, Chinese Academy of Sciences, Beijing 100083, China

ABSTRACT: ZnO nanorods (NRs) and nanosheets (NSs) were fabricated by adjusting the growth orientation of ZnO crystals in the reaction solution, respectively. The thin ZnO NSs were slowly assembled on the surface of NRs to form a hierarchically structured NR–NS photoelectrode for constructing CdS/CdSe quantum-dot-sensitized solar cells (QDSCs). This hierarchical structure had two advantages in improving the power conversion efficiency (PCE) of the solar cells: (a) it increased the surface area and modified the surface profile of the ZnO NRs to aid in harvesting more quantum dots, which leads to a high short-current density (J_{sc}); (b) it facilitated transportation of the electrons in this compact structure to reduce the charge recombination, which led to enhancement of the open-circuit voltage (V_{oc}) and fill factor (FF). As a result, the QDSC assembled with the hierarchical NR–NS photoelectrode exhibited a high PCE of 3.28%, which is twice as much as that of the NR photoelectrode (1.37%).

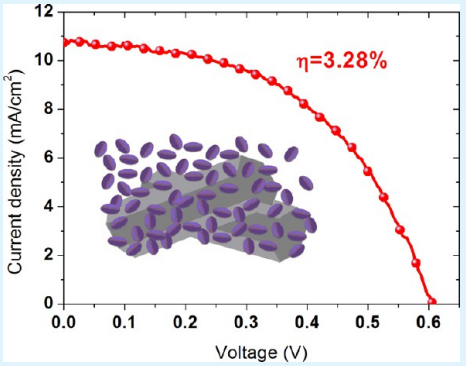

KEYWORDS: *quantum-dot-sensitized solar cell, ZnO, CdS/CdSe, nanorod, nanosheet*

1. INTRODUCTION

The establishment of low-cost and high-performance solar cells for sustainable energy sources to replace fossil fuels has become an urgent subject imposed on scientists around the world.[1,2] As a cost-effective alternative to silicon-based photovoltaics, quantum-dot-sensitized solar cells (QDSCs) have attracted considerable attention recently and shown promising development for next-generation solar cells.[2−6] QDSCs can be regarded as derivatives of dye-sensitized solar cells (DSCs), which were first reported by Oregan and Greatzel in 1991.[7] However, QDSCs use semiconductor quantum dots (QDs)[8−11] as the photosensitizer instead of organic dyes because of their versatile optical and electrical properties, such as (1) tunable band gap depending on the QD size, (2) larger extinction coefficient, (3) high stability toward water and oxygen, and (4) generation of multiple excitons with single-photon absorption.[12−14] The theoretical photovoltaic conversion efficiency of a QDSC can reach up to 44% in view of the multiple exciton generation of QDs.[14,15]

Among the various QDs that are used for QDSCs, CdS and CdSe are attractive owing to their high potential for light harvesting in the visible-light region.[12,16] CdSe has a band gap of 1.7 eV and may therefore absorb photons with wavelengths shorter than 700 nm and shows better performance compared to CdS.[17] However, it was found that CdSe is difficult to deposit directly on oxides such as TiO_2 and ZnO. For this reason, modification of oxides with CdS has usually been adopted to improve the adsorption of CdSe.[18,19] Another reason that CdS has been used is to induce CdS/CdSe cosensitization, which broadens the optical absorption of the solar cells. So far, CdS/CdSe-cosensitized QDSCs have reached power conversion efficiencies (PCEs) higher than 4%.[10,20] We synthesized CdS and CdSe QDs within TiO_2 and ZnO mesoporous films to assemble CdS/CdSe-cosensitized solar cells by successive ionic layer absorption and reaction (SILAR) and chemical bath deposition (CBD), respectively, both of which showed high efficiency.[14,21−23] Most recently, Santra and Kamat reported that QDSC with manganese-doped CdS/CdSe achieved a PCE of 5.4%.[3]

As a wide-band-gap semiconductor for the sensitizer scaffold, conventional TiO_2 and ZnO porous nanocrystalline films had been used in both DSCs and QDSCs. Our previous research reported[14] that QDs had difficultly entering the inner pores of the films in comparison with organic dyes, ultimately leading to several issues: (1) direct exposure of the oxide film in the electrolyte, resulting in a serious degree of recombination between the electrons in the oxide and holes in the electrolyte; (2) less QD loading in the films. Open structures, such as nanorods (NRs), nanowires (NWs), and nanotubes, can facilitate the distribution of QDs from the surface to the interior of the films and enhance the QD loading. ZnO is considered an excellent candidate material as a photoelectrode because of its high electron mobility.[24−26] In addition, ZnO can easily form anisotropic structures such as NRs and NWs. For

Received: January 11, 2014
Accepted: February 28, 2014
Published: February 28, 2014

   dx.doi.org/10.1021/am500209f | ACS Appl. Mater. Interfaces 2014, 6, 4466−4472

the structure of ZnO NRs, ZnO can serve as the backbone for direct electron transport by providing short transport distances. Some studies have already demonstrated the use of ZnO NRs and NWs for application in QDSCs.[27−32] However, QDSCs based on 1D structures (NRs and NWs) have not reached as high of conversion efficiencies as expected, likely because of their low surface areas, leading to diminished QD loadings. The hierarchical structures of ZnO NRs assembled with nanoparticles or nanosheets (NSs) have been identified as an effective means of enhancing the DSC performance.[33] Although QDSCs have somewhat different structure than DSCs, the method of assembling the hierarchically structured photoelectrode is accredited to be effective in improving the performance of QDSCs.

In this work, we designed a hierarchically structured ZnO photoelectrode assembled with NRs and NSs. It is anticipated that the resulting hierarchical configuration would enhance the available surface area for accommodating more QDs, which could increase both the short-circuit current density (J_{sc}) and the open-circuit voltage (V_{oc}) as well as the overall fill factor (FF) of the solar cells. As a result, the PCE of the QDSCs increases from 1.37% for ZnO NRs to 3.28% for the hierarchically structured ZnO photoelectrode.

2. EXPERIMENTAL METHODS

2.1. Experimental Process. Figure 1 illustrates the formation steps of the hierarchically structured ZnO photoelectrode for QDSCs.

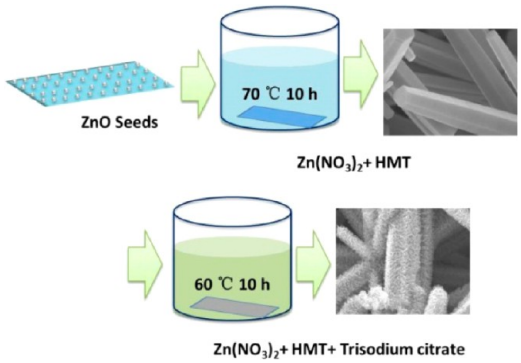

Figure 1. Schematic of the synthesis process of hierarchically structured ZnO NRs−NSs.

First, a seed layer of ZnO was deposited on indium-doped tin oxide (ITO) glass from which the ZnO NRs were grown in a solution of $Zn(NO_3)_2$ and hexamethylenetetramine (HMT) at 70 °C; the ZnO NRs were grown along the (0001) plane and overlaid onto the ITO substrate. Finally, the ZnO NRs were coated with ZnO NSs of small size in a secondary reaction solution that incorporated $Zn(NO_3)_2$, HMT, and trisodium citrate.

2.2. Preparation of ZnO NRs. The ITO substrates were spin-coated with 0.60 M zinc acetate in a solution of 2-methoxyethanol and monoethanolamine to form a seed layer of ZnO, followed by heat treatment at 300 °C for 10 min. The ZnO NRs were prepared on the seeded ITO glass substrate by solution reaction in a 0.015 M zinc nitrate and HMT aqueous solution as reported previously.[23,33] The seeded ITO glass was placed in the aqueous solution, and the solution reaction was carried out at 70 °C for 10 h. Then, the ZnO NR-coated substrate was taken out and dried at 70 °C. The as-received substrate underwent a sintering process in air at 350 °C for 30 min.

2.3. Formation of Hierarchically Structured ZnO NRs−NSs. The ZnO NRs were immersed in an aqueous solution of 0.01 M zinc nitrate, 0.01 M HMT, and 0.001 M trisodium citrate at 60−70 °C for 10 h. The substrate was drained from the reaction solution and washed several times with deionized water. The substrate was then calcined at 350 °C for 30 min.

2.4. Fabrication of CdS/CdSe-Sensitized Solar Cells. For the growth of CdS QDs, the substrates were first immersed in a 0.1 M cadmium nitrate [$Cd(NO_3)_2$] and methanol solution for 1 min. Successively, the substrates were dipped into a 0.1 M sodium sulfide (Na_2S) and methanol solution for another 1 min to allow S^{2-} to react with the preadsorbed Cd^{2+}, leading to the formation of CdS. This procedure was denoted as one SILAR cycle. In total, five SILAR cycles were employed to obtain a suitable amount of CdS on the TiO_2 film. In a subsequent step, CdSe was deposited on the CdS-coated substrates through a CBD method. In brief, 0.1 M sodium selenosulfate (Na_2SeSO_3), 0.1 M cadmium acetate [$Cd(CH_2COO)_2$], and 0.2 M trisodium salt of nitrilotriacetic acid [$N(CH_2COONa)_3$] were mixed together with a 1:1:1 volume ratio. The CdS-coated substrates were then vertically immersed into the solution for deposition of the CdSe layer under dark conditions at 24 °C for 3 h. After CdSe deposition, a ZnS passivation layer was deposited with two SILAR cycles by soaking the substrate in an aqueous solution containing 0.1 M zinc nitrate and 0.1 M sodium sulfide, which acted as Zn^{2+} and S^{2-} sources, respectively. The electrolyte employed in this study was composed of 1 M S and 1 M Na_2S in deionized water. The counter electrode was a Cu_2S film fabricated on brass foil. The preparation of the Cu_2S electrode can be described as follows: brass foil was immersed in 37% HCl at 70 °C for 5 min, then rinsed with water, and dried in air. Following this step, the etched brass foil was dipped in a 1 M S and 1 M Na_2S aqueous solution, resulting in a black Cu_2S layer forming on the foil.

2.5. Characterization. The morphology of the ZnO NRs−NSs was characterized by scanning electron (SEM; JSM-7000) and transmission electron (TEM; Tecnai G2 F20) microscopy. Nitrogen sorption isotherms were measured using a Quantachrome NOVA 4200e. Samples are degassed at 250 °C under vacuum for at least 6 h prior to measurement. The multipoint Brunauer−Emmett−Teller (BET) method was used to determine the specific surface area. The photovoltaic properties were measured using an HP 4155A programmable semiconductor parameter analyzer under AM 1.5 simulated sunlight with a power density of 100 mW/cm^2. The cell area is 0.25 cm^2. Optical absorption (Perkin-Elmer Lambda 900 UV/vis/IR spectrometer) was used to study the light absorption properties of the samples. Electrochemical impedance spectroscopy (EIS) was carried out using a Solartron 1287A coupled with a Solartron 1260 FRA/impedance analyzer to investigate the electronic and ionic processes in QDSCs.

3. RESULTS AND DISCUSSION

Figure 2a shows the SEM image of the cross section of the ZnO NR film on the ITO glass, indicating that the thickness is around 15 μm. The inset in Figure 2a shows the NRs lying on the seeded layer, which increases the adhesive strength between the NRs and ITO substrate to improve electron transport at their interface. Parts b and c of Figure 2 display the low- and high-resolution SEM images of the ZnO NRs, respectively. It can be seen that the average length and diameter of the NRs are ∼10 μm and ∼600 nm, respectively. The large gaps and pores among the NRs are helpful for achieving thorough penetration of the CdS/CdSe QDs (3−10 nm)[14] into the ZnO NR photoelectrode film. The ZnO NRs were synthesized in a solution of HMT and $Zn(NO_3)_2$ at 70 °C. HMT acts as a pH buffer, which controls the supply quantity of OH^- to keep the low concentration of OH^- in the solution. Under this condition, ZnO crystals grow fast along the *c*-axis direction because of the high surface energy of the polar (001) plane for adsorbing more OH^-.[34] When the citrate ions were added in the solution of $ZnNO_3$ and HMT, the crystal growth along ⟨001⟩ orientations was suppressed to form short and fat hexagonal crystals (NSs). So, the NSs deposit gradually from a

dx.doi.org/10.1021/am500209f | ACS Appl. Mater. Interfaces 2014, 6, 4466−4472

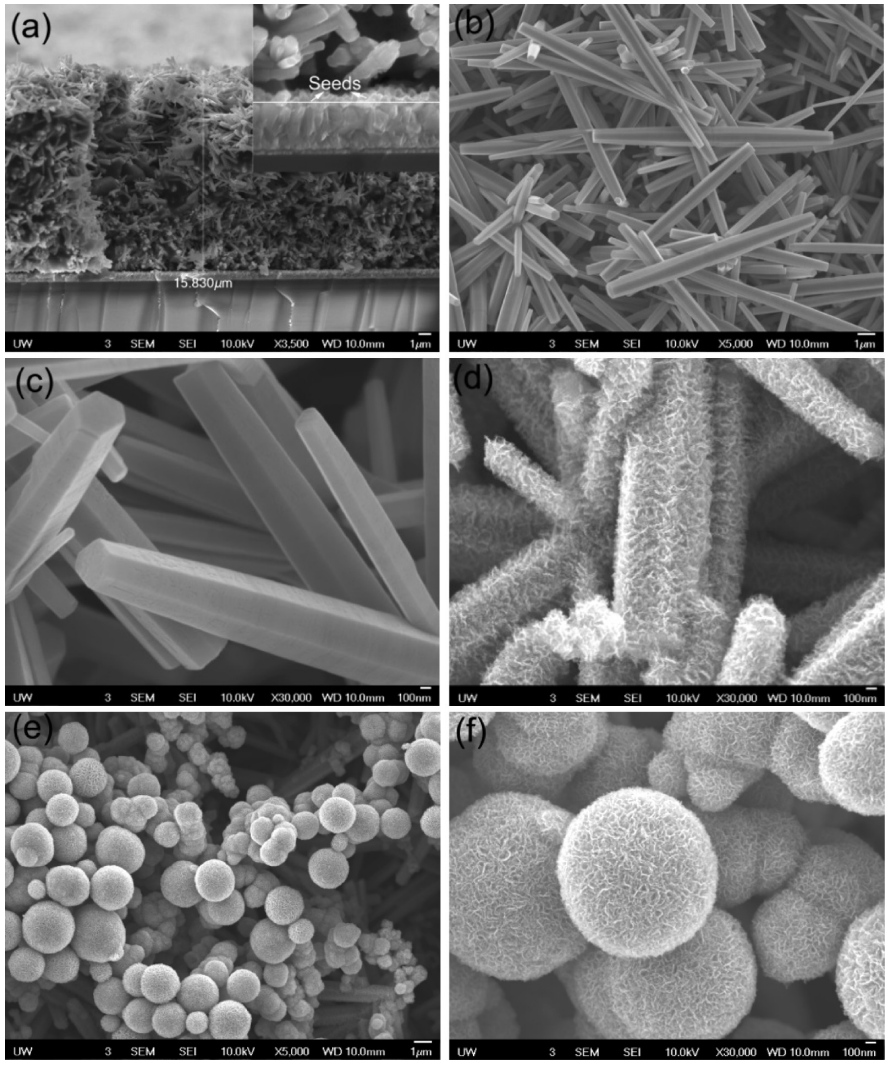

Figure 2. (a) SEM images of the cross section of the ZnO NR film. The inset shows the cross section of the seed layer and NR film. (b and c) SEM images of ZnO NRs and of ZnO NRs−NSs synthesized at (d) 60 and (e and f) 70 °C.

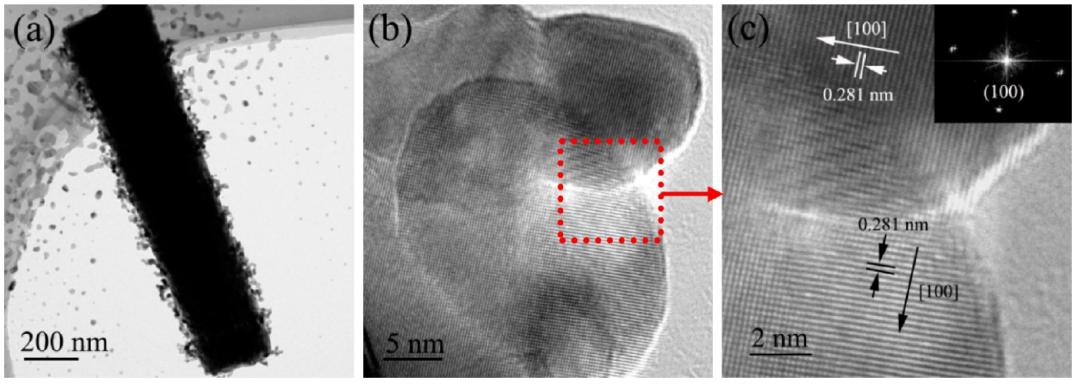

Figure 3. (a) TEM and (b and c) HRTEM images of the ZnO NRs−NSs. The inset shows the NSs FFT diffraction pattern.

supersaturation solution and deposit on the surface of NRs. As displayed in Figure 2d, the smooth surfaces of the NRs became "rough" and were surrounded by NSs, effectively forming a "shell". During the synthesis process of NSs, too high of synthesis temperature (≥70 °C) can drive the NSs to assemble and form nanospheres, as shown in Figure 2e,f. It has been reported[35] that large numbers of NSs would form quickly in the solution and then attach to each other to form microspheres in the reaction solution at too high of temperature. The nanospherical structure was determined to not be beneficial for the loading of QDs because it attenuated electron transport compared with the NR−NS hierarchical structure.

Parts a and b of Figure 3 show the TEM and high-resolution TEM (HRTEM) images of the ZnO NRs−NSs, respectively, revealing that the ZnO NR is surrounded by small NSs 10−15 nm in size. As displayed in Figure 3c and the corresponding

dx.doi.org/10.1021/am500209f | ACS Appl. Mater. Interfaces 2014, 6, 4466−4472

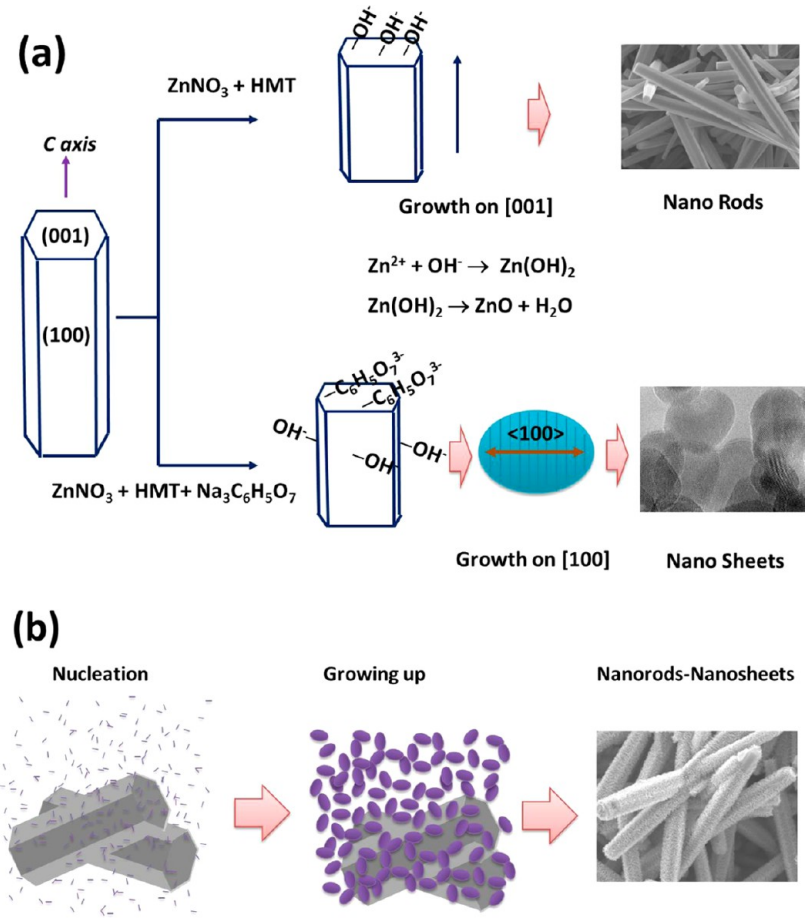

Figure 4. Schematics of (a) the growth mechanism for ZnO NR and NS in different reaction solutions. (b) Proposed formation mechanism of the hierarchical structure of ZnO NRs–NSs.

inset, the lattice constant and fast Fourier transform (FFT) diffraction pattern demonstrate that the NS exhibits a single-crystalline phase with the (100) plane, indicating that the fastest growth direction for the ZnO crystal is ⟨100⟩ during the synthesis process. Although the synthesis mechanism of the NRs–NSs is not entirely clear, a schematic of the proposed formation mechanism of NR and NS is illustrated in Figure 4. It has been proposed that HMT reacts with water to produce ammonia, which, in turn, reacts with water to generate OH^-.[33,36] HMT can keep a low supersaturation reaction environment of reacting Zn^{2+} with OH^- for ZnO crystals. The chemistry of the process is summarized as follows:[37]

$$C_6H_{12}N_4 + 6H_2O \rightarrow 6CH_2O + 4NH_3 \quad (1)$$

$$NH_3 + H_2O \rightarrow NH_4^+ + OH^- \quad (2)$$

$$Zn^{2+} + 4OH^- \rightarrow Zn(OH)_4^{2-} \quad (3)$$

$$Zn(OH)_4^{2-} \rightarrow Zn(OH)_2 + 2OH^- \quad (4)$$

$$Zn(OH)_2 \rightarrow ZnO + 2H_2O \quad (5)$$

It has been reported[22,34,37] that ⟨001⟩ is the preferred growth direction of ZnO crystals in a reaction solution of $Zn(NO_3)_2$ and HMT because of the high surface energy of the (001) plane. As shown in Figure 4a, OH^- ions are preferably adsorbed on the (001) plane of ZnO, leading to ZnO crystals growing along the fastest orientation, the *c* axis ⟨001⟩. Previous research[38] has studied the effect of citrate ions on ZnO crystal morphology, which reported that the citrate molecules were preferentially adsorbed onto the (001) surface and thus inhibited crystal growth along the ⟨001⟩ orientations. As displayed in Figure 4a, we deduced that citrate ions ($C_6H_5O_7^{3-}$) preferably concentrated on the (001) plane because of the high surface energy. So, more ions of OH^- were adsorbed on the other plane (100) than on the (001). ZnO crystal growth along the ⟨001⟩ orientations was suppressed, but crystals were still able to grow sideways (such as the ⟨100⟩ direction) in the form of thin sheets. As determined from the FFT diffraction pattern from the corresponding HRTEM image, the crystals are prone to grow along the ⟨100⟩ direction. This conclusion is consistent with ref 26 about the role of the citrate ions. Figure 4b is a schematic illustration of the formation mechanism of the hierarchical structure of ZnO NRs–NSs. There is high surface energy and more defects on the surface of ZnO NRs, which is helpful for the nucleation and growth of ZnO NSs. So, the ultrathin NSs are highly flexible and thus can readily deposit onto the surface of the ZnO NRs, forming the hierarchical structure.

Figure 5 displays the nitrogen sorption isotherms, indicating that the hierarchical NR–NS structure has a much higher BET surface area (31.5 m^2/g) than the ZnO NRs (14.3 m^2/g). Therefore, the assembled NSs on the surface of ZnO NRs can increase the surface area of the photoelectrode film, which is helpful for increasing the load of QDs.

dx.doi.org/10.1021/am500209f | ACS Appl. Mater. Interfaces 2014, 6, 4466–4472

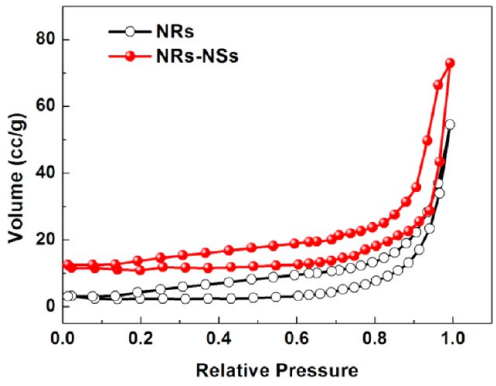

Figure 5. Nitrogen sorption isotherms for the ZnO NRs and hierarchical ZnO NRs−NSs.

Figure 6 shows the TEM and HRTEM images of the ZnO NRs−NSs adsorbed with QDs, revealing that the ZnO NRs−

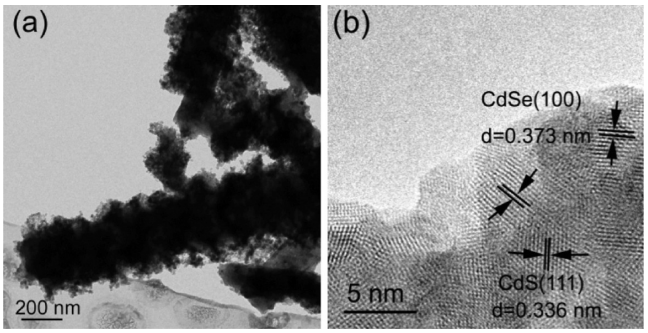

Figure 6. (a) TEM and (b) HRTEM images of the ZnO NRs−NSs loaded with QDs.

NSs are surrounded by small particles 4−6 nm in size. The indexing of the small CdS/CdSe particles can be confirmed by comparing the observed lattice parameters with the data available from the JCPD. The inner layer crystallites have a lattice fringe of 0.336 nm, which is recognized as the (111) plane of CdS (JCPDS 10-0454); the lattice fringe of the outer layer crystallites is 0.373 nm, which is ascribed to the (100) plane of CdSe (JCPDS 08-0459).

The optical absorbance spectra of the ZnO photoelectrodes loaded with QDs are shown in Figure 7. The results reveal that the absorbance of the NRs−NSs is higher than that of the NRs.

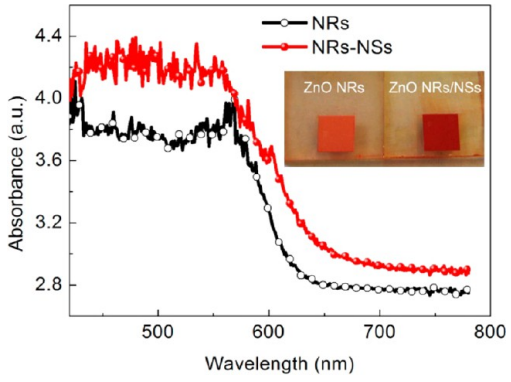

Figure 7. Optical absorbance spectra of the ZnO photoelectrodes loaded with QDs.

The high absorbance of the photoelectrode indicates that a greater amount of QDs can be accommodated. In a comparison of the energy-dispersive spectrometry results of S and Se elements in the photoelectrodes, the mass fractions of S and Se in ZnO NRs−NSs (5.6 wt % for S and 11.2 wt % for Se) are more than those in ZnO NRs (3.3 wt % for S and 8.5 wt % for Se). In addition, the inset image in Figure 7 shows the much darker color of the hierarchical NR−NS sample compared to that of the ZnO NR sample, which also implies that a greater amount of QDs are adsorbed on the former rather than the latter. The previous results may be attributed to (1) changing the surface profile and chemical energy of the photoelectrode by the addition of NSs for harvesting a greater amount of QDs and (2) increasing the surface area of the photoelectrode by deposition of NSs to favor high QD loadings. The more QDs that are loaded within the photoelectrode, the higher the photocurrent density (J_{sc}) that can be obtained.

In addition to enhanced QD loading, the structure of the photoelectrode effectively enhances electron transport, electron lifetime, and charge recombination. In order to evaluate the resistance distribution and charge recombination processes, EIS measurements have been carried out. Figure 8 shows the impedance spectra of the QDSCs measured under forward bias (0.5 V) and dark conditions. In Figure 8a, the semicircles correspond to electron transfer at the photoelectrode/QDs/electrolyte interface and transport in the photoelectrode (R_{ct}), respectively.[39] A fitting result of the impedance spectra is listed in Table 1. Compared to the ZnO NRs, R_{ct} of the ZnO NR−NS structure increases from 66.4 to 101.2 Ω/cm^2; R_{ct} can be considered as the charge recombination under dark conditions.[40] Thus, the results indicate that electrons in the structured ZnO NR−NS photoelectrode are more difficult to recombine with the electrolyte redox couple (S^{2-}/S_n^{2-}) in view of the high R_{ct} value. The increase in R_{ct} of the ZnO NRs−NSs is possibly attributed to the compact structure of the hierarchical photoelectrode. Figure 8d shows the structure of two photoelectrodes. Compared to the ZnO NRs, the structure of ZnO NRs−NSs becomes compact and the gaps between ZnO and ITO decrease. For yielding electron−hole pairs from QDs, they are rapidly separated into electrons and holes at the interface between ZnO and QDs. The electrons are injected into ZnO, and holes are released by redox couples (S^{2-}/S_n^{2-}) in the electrolyte. So, electrons in the compact ZnO NR−NS hierarchical structure are easily transported to the counter electrode rather than back into the electrolyte. Figure 8b shows the Bode plots of QDSCs with different photoelectrode structure. The curve peak of the spectrum can be used to determine the electron lifetime in ZnO according to eq 6.[41]

$$\tau_n = 1/2\pi f_{min} \quad (6)$$

As presented in Table 1, the electron lifetime of the hierarchically structured photoelectrode device is up to 4.7 ms, which is approximately 2 times that of the ZnO NR device (2.9 ms). In other words, the electron lifetime in the conduction band is prolonged because of a decrease in the charge recombination. It is well-known that the charge recombination and electron lifetime have a direct impact on V_{oc}, FF, and PCE for DSCs, and the same applies for QDSCs. V_{oc} can be expressed by eq 7:[42,43]

$$V_{oc} = (RT/\beta F)\ln\{AI/(n_0 k_b[S_n^-] + n_0 k_r[D^+])\} \quad (7)$$

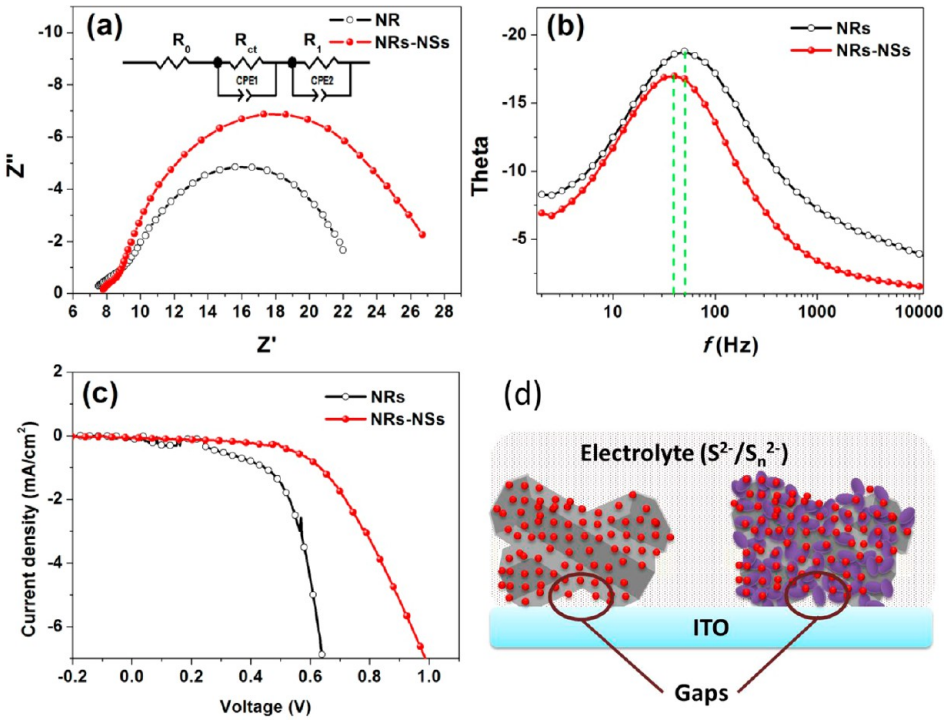

Figure 8. (a) Nyquist and (b) Bode plots of the QDSCs under forward bias (0.5 V). (c) $J-V$ curves of the QDSCs under dark conditions. (d) Schematics of the photoelectrode structure.

Table 1. EIS Results of QDSCs

photoelectrode	R_{ct} (Ω/cm^2)	τ (mS)
NRs	66.4	2.9
NRs–NSs	101.2	4.7

where R is the molar gas constant, T is the temperature, F is the Faraday constant, β is the reaction order for S_n^- and electrons, A is the electrode area, I is the incident photon flux, n_0 is the concentration of accessible electronic states in the conduction band, and k_b and k_r are the kinetic constants of the back-reaction of the injected electrons with a polysulfide electrolyte and the recombination of these electrons with oxidized QDs (D^+), respectively. Considering that ω_{max} $(1/f_{min})$ is the same as the back-reaction constant (k_b) and that V_{oc} depends logarithmically on f_{min}, it is clear that the V_{oc} value increases with a decrease of the back-reaction constant (same as f_{min}). From Figure 8b, the device with the hierarchically structured photoelectrode has much lower f_{min} than that using the ZnO NR photoelectrode. Subsequently, according to eq 6, the device with the hierarchically structured photoelectrode should have higher V_{oc}. The charge-transfer resistance at the photoelectrode/electrolyte interface, denoted as R_{ct} in Figure 8a, can be considered as part of a shunt resistance (R_{sh}) because it behaves like a diode with the applied bias voltage.[40] R_{sh} relates to FF according to eq 8:[40]

$$FF = FF_0(1 - 1/R_{sh}) \quad (8)$$

where FF_0 is the theoretical maximum FF. R_{sh} is consistent to R_{ct}. From the EIS results, it can be inferred that the increase for the QDSC is a result of an increase in R_{sh}, which enhances FF of the solar cell. Following previous discussions, it is evident that this modification contributes toward improving J_{sc}, FF, and V_{oc} of the QDSCs.

Figure 9 shows the $J-V$ curves for the solar cells measured under the illumination of one sun (AM 1.5, 100 mW/cm^2), and

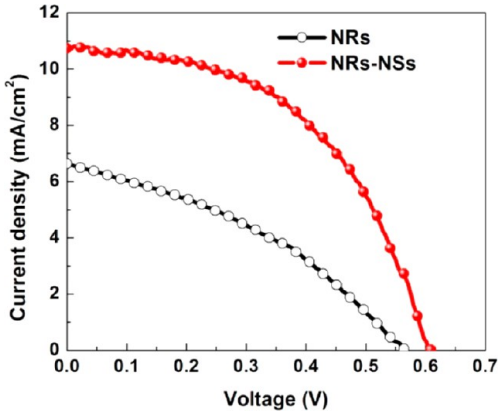

Figure 9. $J-V$ curves of QDSCs assembled with different photoelectrodes under simulated AM 1.5, 100 mW/cm^2 sunlight.

the performance parameters of the solar cells are listed in Table 2. The QDSC assembled with hierarchically structured ZnO exhibits high performance: J_{sc} = 10.74 mA/cm^2, V_{oc} = 0.61 V, FF = 0.50, and PCE = 3.28%. Compared with the ZnO NRs photoelectrode, the hierarchically structured ZnO NR–NS photoelectrode displays increases in V_{oc}, J_{sc}, FF, and PCE by 7%, 62%, 39%, and 139%, respectively. The performance of the

Table 2. Properties of QDSCs Assembled with Different Photoelectrodes

photoelectrode	V_{oc} (V)	J_{sc} (mA/cm^2)	FF	PCE (%)
NRs	0.57	6.62	0.36	1.37
NRs–NSs	0.61	10.74	0.50	3.28

dx.doi.org/10.1021/am500209f | ACS Appl. Mater. Interfaces 2014, 6, 4466–4472

QDSC assembled with ZnO NRs can be enhanced via a chemical synthesis process by introducing a shell of ZnO NSs for increasing the surface area to harvest a greater amount of QDs and reduce the charge recombination.

4. CONCLUSIONS

A hierarchically structured photoelectrode of ZnO NRs−NSs for CdS/CdSe QDSCs was investigated. The ZnO NRs were initially seeded and then grown on ITO using a solution synthesis process at 70 °C. ZnO NSs 10−15 nm in length were slowly assembled on the surface of the NRs in the reaction solution under 60 °C. Compared to ZnO NRs, the hierarchical structure of the NRs−NSs had two advantages for QDSCs: (a) it increased the surface area and modified the surface profile of the ZnO NRs to aid in harvesting more QDs, which leads to a high short-current density (J_{sc}); (b) it facilitated transportation of the electrons in this compact structure to reduce the charge recombination, which led to enhancement of the open-circuit voltage (V_{oc}) and fill factor (FF). As a result, the solar cells assembled with the hierarchically structured ZnO photoelectrode displayed high performance under AM 1.5 simulated sunlight with a power density of 100 mW/cm^2, J_{sc} of 10.74 mA/cm^2, V_{oc} of 0.61 V, FF of 0.50, and PCE of 3.28%.

AUTHOR INFORMATION

Corresponding Authors

*E-mail: tianjianjun@mater.ustb.edu.cn.

*E-mail: gzcao@u.washington.edu.

Notes

The authors declare no competing financial interest.

ACKNOWLEDGMENTS

This work was supported by the National Science Foundation of China (Grants 51374029 and 51174247) and Program for New Century Excellent Talents in University (Grant NCET-13-0668). This work was also supported in part by the National Science Foundation (Grant DMR 1035196), the University of Washington TGIF grant, and the Royalty Research Fund from the Office of Research at the University of Washington.

REFERENCES

(1) Graetzel, M.; Janssen, R. A. J.; Mitzi, D. B.; Sargent, E. H. *Nature* **2012**, *488*, 304−312.

(2) Tada, H.; Fujishima, M.; Kobayashi, H. *Chem. Soc. Rev.* **2011**, *40*, 4232−4243.

(3) Santra, P. K.; Kamat, P. V. Mn-Doped Quantum Dot Sensitized Solar Cells: A Strategy to Boost Efficiency over 5%. *J. Am. Chem. Soc.* **2012**, *134*, 2508−2511.

(4) Hossain, M. A.; Jennings, J. R.; Koh, Z. Y.; Wang, Q. *ACS Nano* **2011**, *5*, 3172−3181.

(5) Ryu, J.; Lee, S. H.; Nam, D. H.; Park, C. B. *Adv. Mater.* **2011**, *23*, 1883−1888.

(6) Sugaya, T.; Numakami, O.; Oshima, R.; Furue, S.; Komaki, H.; Amano, T.; Matsubara, K.; Okano, Y.; Niki, S. *Energy Environ. Sci.* **2012**, *5*, 6233−6237.

(7) Oregan, B.; Greatzel, M. *Nature* **1991**, *353*, 737−740.

(8) Bang, J. H.; Kamat, P. V. *Adv. Funct. Mater.* **2010**, *20*, 1970−1976.

(9) Gonzalez-Pedro, V.; Xu, X.; Mora-Sero, I.; Bisquert, J. *ACS Nano* **2010**, *4*, 5783−5790.

(10) Yu, X.-Y.; Liao, J.-Y.; Qiu, K.-Q.; Kuang, D.-B.; Su, C.-Y. *ACS Nano* **2011**, *5*, 9494−9500.

(11) Cheng, C. W.; Karuturi, S. K.; Liu, L. J.; Liu, J. P.; Li, H. X.; Su, L. T.; Tok, A. I. Y.; Fan, H. J. *Small* **2012**, *8*, 37−42.

(12) Zhu, G.; Pan, L.; Xu, T.; Sun, Z. *ACS Appl. Mater. Interfaces* **2011**, *3*, 3146−3151.

(13) Lee, Y. L.; Lo, Y. S. *Adv. Funct. Mater.* **2009**, *19*, 604−609.

(14) Tian, J. J.; Gao, R.; Zhang, Q. F.; Zhang, S. G.; Li, Y. W.; Lan, J. L.; Qu, X. H.; Cao, G. Z. *J. Phys. Chem. C* **2012**, *116*, 18655−18662.

(15) Li, T. L.; Lee, Y. L.; Teng, H. *Energy Environ. Sci.* **2012**, *5*, 5315−5324.

(16) Lee, Y. H.; Im, S. H.; Chang, J. A.; Lee, J. H.; Seok, S. I. *Org. Electron.* **2012**, *13*, 975−979.

(17) Hossain, M. A.; Jennings, J. R.; Shen, C.; Pan, J. H.; Koh, Z. Y.; Mathews, N.; Wang, Q. *J. Mater. Chem.* **2012**, *22*, 16235−16242.

(18) Chong, L.-W.; Chien, H.-T.; Lee, Y.-L. *J. Power Sources* **2010**, *195*, 5109−5113.

(19) Zarazua, I.; De la Rosa, E.; Lopez-Luke, T.; Reyes-Gomez, J.; Ruiz, S.; Angeles Chavez, C.; Zhang, J. Z. *J. Phys. Chem. C* **2011**, *115*, 23209−23220.

(20) Zhang, Q.; Guo, X.; Huang, X.; Huang, S.; Li, D.; Luo, Y.; Shen, Q.; Toyoda, T.; Meng, Q. *Phys. Chem. Chem. Phys.* **2011**, *13*, 4659−4667.

(21) Tian, J. J.; Zhang, Q. F.; Uchaker, E.; Gao, R.; Qu, X. H.; Zhang, S. G.; Cao, G. Z. *Energy Environ. Sci.* **2013**, *6*, 3542−3547.

(22) Tian, J. J.; Zhang, Q. F.; Uchaker, E.; Liang, Z. Q.; Gao, R.; Qu, X. H.; Zhang, S. G.; Cao, G. Z. *J. Mater. Chem. A* **2013**, *1*, 6770−6775.

(23) Tian, J. J.; Zhang, Q. F.; Zhang, L. L.; Gao, R.; Shen, L. F.; Zhang, S. G.; Qu, X. H.; Cao, G. Z. *Nanoscale* **2013**, *5*, 936−943.

(24) Chou, T. P.; Zhang, Q. F.; Fryxell, G. E.; Cao, G. Z. *Adv. Mater.* **2007**, *19*, 2588−2592.

(25) Zhang, Q. F.; Cao, G. Z. *J. Mater. Chem.* **2011**, *21*, 6769−6774.

(26) Zhang, Q. F.; Chou, T. R.; Russo, B.; Jenekhe, S. A.; Cao, G. Z. *Angew. Chem., Int. Ed.* **2008**, *47*, 2402−2406.

(27) Seol, M.; Kim, H.; Tak, Y.; Yong, K. *Chem. Commun.* **2010**, *46*, 5521−5523.

(28) Seol, M.; Ramasamy, E.; Lee, J.; Yong, K. *J. Phys. Chem. C* **2011**, *115*, 22018−22024.

(29) Yao, C.-Z.; Wei, B.-H.; Meng, L.-X.; Li, H.; Gong, Q.-J.; Sun, H.; Ma, H.-X.; Hu, X.-H. *J. Power Sources* **2012**, *207*, 222−228.

(30) Bora, T.; Kyaw, H. H.; Dutta, J. *Electrochim. Acta* **2012**, *68*, 141−145.

(31) Li, L.-B.; Wang, Y.-F.; Rao, H.-S.; Wu, W.-Q.; Li, K.-N.; Su, C.-Y.; Kuang, D.-B. *ACS Appl. Mater. Interfaces* **2013**, *5*, 11865−11871.

(32) Liao, J.-Y.; He, J.-W.; Xu, H.; Kuang, D.-B.; Su, C.-Y. *J. Mater. Chem.* **2012**, *22*, 7910−7918.

(33) Dong, H. P.; Wang, L. D.; Gao, R.; Ma, B. B.; Qiu, Y. *J. Mater. Chem.* **2011**, *21*, 19389−19394.

(34) Cao, B.; Cai, W. *J. Phys. Chem. C* **2008**, *112*, 680−685.

(35) Gao, R.; Tian, J.; Liang, Z.; Zhang, Q.; Wang, L.; Cao, G. *Nanoscale* **2013**, *5*, 1894−1901.

(36) Wu, C. T.; Liao, W. P.; Wu, J. J. *J. Mater. Chem.* **2011**, *21*, 2871−2876.

(37) Zhou, Z.; Deng, Y. *J. Phys. Chem. C* **2009**, *113*, 19853−19858.

(38) Tian, Z. R. R.; Voigt, J. A.; Liu, J.; McKenzie, B.; McDermott, M. J.; Rodriguez, M. A.; Konishi, H.; Xu, H. F. *Nat. Mater.* **2003**, *2*, 821−826.

(39) Koide, N.; Islam, A.; Chiba, Y.; Han, L. Y. *J. Photochem. Photobiol., A* **2006**, *182*, 296−305.

(40) Park, K.; Zhang, Q. F.; Garcia, B. B.; Cao, G. Z. *J. Phys. Chem. C* **2011**, *115*, 4927−4934.

(41) Kern, R.; Sastrawan, R.; Ferber, J.; Stangl, R.; Luther, J. *Electrochim. Acta* **2002**, *47*, 4213−4225.

(42) Wang, Q.; Ito, S.; Gratzel, M.; Fabregat-Santiago, F.; Mora-Sero, I.; Bisquert, J.; Bessho, T.; Imai, H. *J. Phys. Chem. B* **2006**, *110*, 25210−25221.

(43) Lee, K.; Park, S. W.; Ko, M. J.; Kim, K.; Park, N. G. *Nat. Mater.* **2009**, *8*, 665−671.